Biosensors and Bioelectronics 96 (2017) 178–185

Contents lists available at ScienceDirect

Biosensors and Bioelectronics

journal homepage: www.elsevier.com/locate/bios

Carbohydrate-based electrochemical biosensor for detection of a cancer biomarker in human plasma

Marion Devillers, Lama Ahmad, Hafsa Korri-Youssoufi*, Laurent Salmon*

Equipe de Chimie Bioorganique et Bioinorganique, Institut de Chimie Moléculaire et des Matériaux d'Orsay (ICMMO), Univ Paris-Saclay, Univ Paris-Sud, CNRS UMR8182, LabEx LERMIT, rue du doyen Georges Poitou, F-91405 Orsay, France

A B S T R A C T

Autocrine motility factor (AMF) is a tumor-secreted cytokine that stimulates tumor cell motility in vitro and metastasis in vivo. AMF could be detected in serum or urine of cancer patients with worse prognosis. Reported as a cancer biomarker, AMF secretion into body fluids might be closely related to metastases formation. In this study, a sensitive and specific carbohydrate-based electrochemical biosensor was designed for the detection and quantification of a protein model of AMF, namely phosphoglucose isomerase from rabbit muscle (RmPGI). Indeed, RmPGI displays high homology with AMF and has been shown to have AMF activity. The biosensor was constructed by covalent binding of the enzyme substrate D-fructose 6-phosphate (F6P). Immobilization was achieved on a gold surface electrode following a bottom-up approach through an aminated surface obtained by electrochemical patterning of ethylene diamine and terminal amine polyethylene glycol chain to prevent non-specific interactions. Carbohydrate-protein interactions were quantified in a range of 10 fM to 100 nM. Complex formation was analyzed through monitoring of the redox couple Fe^{2+}/Fe^{3+} by electrochemical impedance spectroscopy and square wave voltammetry. The F6P-biosensor demonstrates a detection limit of 6.6 fM and high selectivity when compared to other non-specific glycolytic proteins such as D-glucose-6-phosphate dehydrogenase. Detection of protein in spiked plasma was demonstrated and accuracy of 95% is obtained compared to result obtained in PBS (phosphate buffered saline). F6P-biosensor is a very promising proof of concept required for the design of a carbohydrate-based electrochemical biosensor using the enzyme substrate as bioreceptor. Such biosensor could be generalized to detect other protein biomarkers of interest.

1. Introduction

Cancer is a major cause of mortality in economically developed and developing countries. Thus development of efficient diagnostic tools is the subject of intensive research. The discovery of efficient tumor markers and the approach of their detection is important in the case of diagnosis and therapy approaches. Various cancer biomarkers are now well known and demonstrate high efficacy in prognostic of some cancers, including proteins, antigens, hormones, receptors, genetic markers, and microRNAs (Füzéry et al., 2013). Most biomarkers currently in use are cell surface or secreted proteins (Brooks, 2012), such as prostate specific antigen (PSA), interleukin 6 (IL-6), interleukin 8 (IL-8), carcino-embryonic antigen (CEA), cancer antigens (CA-125, CA15-3, CA19-9, CA27-29), c-reactive protein (CRP), p53 protein, thyroglobuline, and α-fetoprotein (AFP) (Chikkaveeraiah et al., 2012).

Autocrine motility factor (AMF) is an extracellular protein which has the properties of stimulating the active migration of tumor cells in an autocrine manner (Liotta et al., 1986; Watanabe et al., 1996). AMF has been described to have anti-apoptotic activity (Haga et al., 2003; Yanagawa et al., 2004), and to act in a paracrine manner for endothelial cells as an angiogenic factor (Funasaka et al., 2001). Interaction of AMF with the tumor cell receptor AMFR/gp78 is known as a crucial parameter in tumor cells motility in vitro and metastases development in vivo (Watanabe et al., 1991). It is clearly established that over-expression of AMF and/or its receptor AMFR/gp78 is associated to numerous types of cancers (Chiu et al., 2008) including breast (Baumann et al., 1990; Bodansky, 1954a; Jiang et al., 2006; Talukder et al., 2000), kidney (Baumann et al., 1990), gastrointestinal (Baumann and Brand, 1988; Gong et al., 2005; Huang et al., 2014), colorectal (Filella et al., 1991; Paschos et al., 2009; Tsutsumi et al., 2009), pancreatic (Tsutsumi et al., 2004), bladder (Guirguis et al., 1988), prostate (Schwartz et al., 1963), bone and soft tissue (Dobashi et al., 2006), hepatocellular (Torimura et al., 2001; Bayo et al., 2014), and lung (Funasaka et al., 2007; Patel et al., 1995; Takanami et al., 1998) cancers, and is closely related to progression and malignancy of tumors. AMF is found in the serum and/or urine of patients in several

* Corresponding authors.
E-mail addresses: hafsa.korri-youssoufi@u-psud.fr (H. Korri-Youssoufi), laurent.salmon@u-psud.fr (L. Salmon).

http://dx.doi.org/10.1016/j.bios.2017.04.031
Received 5 January 2017; Received in revised form 19 April 2017; Accepted 21 April 2017
Available online 23 April 2017

types of cancer and thus has been used as a biomarker of cancer progression (Baumann et al., 1990; Bodansky, 1954a; Filella et al., 1991; Guirguis et al., 1988; Schwartz et al., 1963).

Because time is a critical parameter in anticancer therapy (Iiizumi et al., 2008), the design of an analytical tool which would allow a systematic, fast, sensitive and specific quantification of cancer biomarkers in human fluids could be of high interest for the positive prognosis of patients with cancer. Hence, such a device could contribute to allow early detection of an ongoing metastatic process, as well as easy monitoring of the efficiency of anticancer agents. The analytical methods used to quantify AMF in human fluids include enzymatic (Gracy and Tilley, 1975), colorimetric (Bodansky, 1954b), and immunological (Dai et al., 2010; Dobashi et al., 2006; Fan et al., 2010) methods. However, these methods appear difficult to adapt for a rapid and systematic analysis. Biosensor technology has the potential to provide fast and accurate detection of cancer biomarkers (Bohunicky and Mousa, 2010; Chikkaveeraiah et al., 2012; Li et al., 2012; Tothill, 2009; Yang et al., 2014). Among the numerous devices reported, electrochemical biosensors are known to display excellent sensing performances with low detection limits (LD) in the picomolar or femtomolar ranges, notably when associated with electrochemiluminescence (ECL) (Hao et al., 2012; Jie et al., 2010; Lin et al., 2011; Zhang et al., 2012) or electrochemical impedance spectroscopy (EIS) (Li et al., 2005a, 2005b; Dong et al., 2006; W. Wang et al., 2015a,2015b; D. Wang et al., 2015a,2015b) as detection methods.

When expressed in cell, AMF has the behavior of phosphoglucose isomerase (PGI) (Jeffery, 1999). PGI is the glycolytic enzyme which reversibly interconverts D-glucose 6-phosphate (G6P) and D-fructose 6-phosphate (F6P). Thus AMF and PGI are strictly identical proteins which have the same structure within various functionalities. In order to design a biosensor capable of detecting AMF, we took advantage of intracellular properties of this protein and developed a carbohydrate biosensor based on the immobilization of the enzyme substrate onto the surface of electrode. The interaction of the carbohydrate with the protein was monitored through measuring the electron transfer properties of a redox marker by electrochemical impedance spectroscopy (ESI). Glycobiosensing and glyconanotechnology have made tremendous advances in the area of glycoanalysis (Gerlach et al., 2010; Reichardt et al., 2013; Sánchez-Pomales and Zangmeister, 2011). The association of carbohydrate-based biosensors and ESI displays an advantage for measuring such association as electrochemical impedance spectroscopy is a powerful method to follow affinity interactions, especially when large molecules are attached to the surface of the electrode. Thus the use of carbohydrate–based biosensors using ESI was reported for high-sensitivity detection of bacteria (Guo et al., 2012).

In this work, we report the development of a carbohydrate biosensor for detection of a protein model of the cancer biomarker AMF, namely phosphoglucose isomerase from rabbit muscle (RmPGI) for which AMF activity was indeed demonstrated. The specific recognition element of the biosensor is the enzyme substrate D-fructose 6-phosphate (F6P). A bottom-up strategy for the construction of the biosensor was followed including electrochemical patterning approach through oxidation of ethylene diamine allowing aminated surface and terminal amine polyethylene glycol chain to avoid non-specific interactions. F6P has been covalently linked through a spacer to a gold electrode via stable oxime bonding. The biolayer formation was characterized through contact angle, FT-IR spectroscopy, SEM and AFM. Cyclic voltammetry (CV) measurements were performed to follow a redox process of Fe^{2+}/Fe^{3+} redox couple. Monitoring of the biolayer construction and molecular recognition between the immobilized F6P bioreceptor and the protein in solution were achieved through square wave voltammetry (SWV) and electrochemical impedance spectroscopy (EIS). We demonstrate that the F6P-biosensor represents a successful proof of concept for the design of a carbohydrate electrochemical biosensor based on one single sugar as substrate of enzyme. The biosensor shows fast, efficient and accurate detection properties of RmPGI, a protein model of the cancer biomarker AMF. It might further contribute to the validation of AMF as a major cancer biomarker and also open the way of using such carbohydrate biosensors for other proteins of interest.

2. Experimental section

2.1. Materials and reagents

N-Hydroxysuccinimide (NHS) was purchased from Fluka (Switzerland). Acetonitrile (ACN), ethylene diamine, lithium perchlorate, pentanoic acid, *N*-(3-dimethylaminopropyl)-*N′*-ethylcarbodiimide hydrochloride (EDC), D-fructose 6-phosphate (F6P), bovine serum albumin (BSA), rabbit muscle phosphoglucose isomerase (RmPGI, 358 U·mg protein^{-1}), and *Saccharomyces cerevisiae* glucose-6-phosphate dehydrogenase (*Sc*G6PDH, 237 U mg protein^{-1}) were purchased from Sigma-Aldrich. Phosphate buffered saline (PBS, pH 7.4, 10 mM Na_2HPO_4, 1.8 mM KH_2PO_4, 2.7 mM KCl, 137 mM NaCl), acetate buffer (pH 4.6, 100 mM), and Tris buffer (pH 8.0, 50 mM) were prepared with double distilled water, filtered on 0.22 µm membranes, and stored at 4 °C before use. Human blood plasma samples were purchased from Helena Biosciences Europe (UK). Polyethylene glycol substituted by an amine terminal group (PEG–NH_2), namely 2-[2-(2-ethoxyethoxy)ethoxy] ethylamine (Alliband et al., 2013) and 2-(*tert*-butoxycarbonyl-aminooxy) acetic acid (Miller et al., 2005) were synthesized according to the reported procedures.

2.2. Electrochemical measurements

Electrochemical deposition and characterization were performed using potentiostat BioLogic VMP3 controlled by EC-Lab software. The three-electrode cell was purchased from Basi and consists of a platinum wire as the counter electrode, a gold disk (surface =$2.01 \cdot 10^{-2}$ cm^2) as the working electrode and Ag/AgCl as the reference electrode. The experiments related to electrodeposition were performed in a small volume cell of 0.2 mL purchased from Basi equipped with porous frit that allows connection with the large volume cell where the reference electrode could be placed in a conductive solution to void iR drop. The potential was checked between the two systems where all electrodes are in the same compartment for the control. The gold electrode surface was cleaned by polishing with diamond pate with various thickness and then activated in 0.5 M sulfuric acid solution by scanning the potential between 0.0 and 1.8 V, during ten cycles with the scan rate 100 mV s^{-1}. Cyclic voltammetry (CV) analysis was conducted in PBS with 5 mM $[Fe(CN)_6]^{4-}/[Fe(CN)_6]^{3-}$ species from 0.0 to 0.5 V using a scan rate of 50 mV s^{-1}. Square wave voltammetry (SWV) was conducted in PBS with 5 mM $[Fe(CN)_6]^{4-}/[Fe(CN)_6]^{3-}$ species from 0.0 to 0.5 V using a conditioning time of 180 s, a frequency of 25 Hz, and a modulation amplitude of 20 mV. Electrochemical impedance spectroscopy (EIS) was conducted in PBS with 5 mM $[Fe(CN)_6]^{4-}/[Fe(CN)_6]^{3-}$ species at potential of 0.0 V and with Dc potential of 10 mV using a frequency range from 100 kHz to 0.1 Hz.

2.3. Construction of the F6P-biosensor

Biosensor construction proceeded by electrodeposition of ethylene diamine (EDA) on the gold electrode surface. Electrodeposition was performed by scanning the potential between 0.0 and 0.7 V vs. Ag/AgCl, during 6 cycles with the scan rate of 50 mV s^{-1}. During the reaction, the working and counter electrodes were placed in the low volume cell (Basi) containing an aqueous solution of 1 M EDA and 0.5 M $LiClO_4$. The same electrolyte was placed in the large volume cell with the reference electrode. The concentration of EDA, the number of cycles and the potential range were optimized to obtain a dense monolayer of EDA on the gold surface and to deposit EDA at low potential range (see Supp. Info.

SI.1–1). During the oxidation reaction, amine group of EDA forms a radical cation which reacts with the gold surface following its immobilization as described previously (Adenier et al., 2004). Contrary to previous work where electrodeposition of EDA was performed at high potential range and in organic media, we succeeded here the electrodeposition process of EDA at low potential range in aqueous solution. To avoid non-specific interactions, the gold surface was then modified with polyethylene glycol substituted by an amine terminal group (PEG–NH_2) using the same method. In the same way, electrodeposition conditions of PEG were optimized by testing the surface through adsorption of BSA (see Supp. Info. SI.1–1). The chosen conditions are to scan the potential between 0.0 and 1.1 V vs. Ag/AgCl at a scan rate of 50 mV s^{-1} during ten cycles in a solution of ACN containing 10 mM PEG–NH_2 and 0.5 M $LiClO_4$. This leads to the attachment of PEG on the gold electrode surface. Following these steps, the electrode was stabilized in PBS during 1 h at room temperature. Attachment of D-fructose 6-phosphate was realized through oxyamine link as direct reaction between the amine group on the surface and the aldehyde group of the sugar does not work. Thereafter 2-(*tert*-butoxycarbonylaminooxy) acetic acid was linked to the NH_2 groups of the modified gold surface to provide aminooxy groups on the surface. The reaction was performed by immersing the electrode in PBS containing 10 mM of the acid reagent, 25 mM of EDC and 25 mM of NHS as coupling agent and during 2.5 h at room temperature. Deprotection of the Boc group was achieved using a 2 M hydrochloric acid solution in acetic acid during 2 h at room temperature after optimization step (see Supp. Info. SI.1–1). D-Fructose 6-phosphate was then linked to oxyamine groups by immersing the electrode in a 2 mg mL^{-1} solution of D-fructose 6-phosphate in acetate buffer for 15 h at 50 °C. This reaction was performed according to the strategy reported for immobilization of other unmodified carbohydrates on glass and silicon surfaces (Zhang et al., 2013). Reaction time and temperature were optimized to allow high surface density of carbohydrate-modified surface (see Supp. Info. SI.1–1). Non-bonded residues were successively washed with a PBS solution containing 0.1% of Tween 20 and double distilled water. Saturation of all non-bonded oxyamine functions was achieved by immersion of the electrode into a PBS solution containing 10 mM pentanoic acid, 25 mM EDC, and 25 mM NHS during 5.5 h at room temperature. In the last step, the electrode was dipped in a 100 µM BSA solution in PBS containing 2.5% of Tween 20 for 10 min to prevent non-specific adsorption of the protein on the electrode surface. Non-fixed enzymes were successively washed by a PBS solution containing 0.1% of Tween 20 and double distilled water. Following these steps, the electrode was maintained in a PBS solution until use.

2.4. Protein detection in PBS and plasma

In order to initially validate our concept, commercially available RmPGI has been used as a protein model of AMF. Indeed, RmPGI shows high homology (93%) with human AMF (Lagana et al., 2000, Lagana et al., 2005), particularly at the enzymatic active site (100% homology). Most importantly, commercial RmPGI has been shown to induce motility of tumor cells, and thus has AMF activity (Watanabe et al., 1996; Lagana et al., 2000). Concerning protein detection in PBS, RmPGI was detected and quantified in the range of concentrations varying from 10 fM to 100 nM. ScG6PDH was detected at 100 nM. All protein solutions were prepared in 50 mM Tris buffer at the optimal pH 8.0 for enzyme activities (Noltmann, 1964; Dyson and Noltman, 1968). A volume of 50 µL of protein solution at the desired concentration was added on the biosensor surface and incubated for 1 h at room temperature. The biosensor was then successively washed with a PBS solution containing 0.1% of Tween 20 and double distilled water. Protein detection in human plasma was performed similarly like in PBS using RmPGI in the range of concentrations varying from 1 fM to 10 pM, and ScG6PDH at 100 nM. Human plasma was used without dilution in PBS and was not filtered.

3. Results and discussion

3.1. Design of the F6P-biosensor

D-Fructose 6-phosphate (F6P) was chosen as the bioreceptor because F6P is the enzymatic substrate of PGI. Indeed, it was demonstrated that interaction of the tumor cell receptor AMFR/gp78 with the cytokine AMF involves partial binding of the glycosylated chain of AMFR/gp78 at the G6P-F6P substrate binding site of AMF. Haga et al. formulated the hypothesis that the glycosylated chain of AMFR/gp78 contains a phosphate or a sulfate sugar recognized by AMF and that the recognition mechanism of the PGI substrate is the primary factor in the AMF–AMFR interaction (Haga et al., 2006). Regioselective binding of F6P has been determined from the deposited tridimensional X-ray crystal structure of RmPGI complexed with its substrate F6P (PDB ID 1HOX) (Lee et al., 2001). The active site structure shows that F6P binds preferentially to the enzyme in its cyclic form, namely β-D-fructofuranose 6-phosphate, and that the only accessible F6P functional group for covalent linkage is the hydroxyl group of carbon 2 (C–2). Therefore, we chose this position for covalent linkage of the recognition sugar in the design of the F6P-biosensor.

The overall biosensor construction involves various steps (Fig. 1). Modification of the surface was monitored by contact-angle measurements, FT-IR spectroscopy analysis, SEM and AFM images and electrochemical analysis. The first step consists in functionalization of the gold surface. Electrodeposition of ethylene diamine (EDA) molecules introduces amino groups onto the surface (Adenier et al., 2004). This reaction was optimized in order to obtain a dense aminated stable surface (See Supp. Info. SI.1–1, Fig. S1–1 and S1-2). It was followed by electrodeposition of polyethylene glycol substituted by a terminal amino group (PEG–NH_2) to allow surface blocking effect for non-specific interactions (See Supp. Info. SI.1–1, Fig. S1–3). Initially, the activated gold electrode displayed a contact angle of 53 ± 1°. Following functionalization with amino groups (step 1), the surface gave an angle of 7 ± 1°, in accord with increasing of surface hydrophilic property due to the presence of protonated amino groups ($-NH_3^+$). Electrodeposition of PEG-NH_2 restores hydrophobicity of the surface leading to an increase of the contact angle to 44 ± 1° (See Supp. Info. SI.1–2, Fig. S1–4). FT-IR spectroscopy underlines the deposition of EDA on the surface as an intense band at 3200 cm^{-1} related to the stretching vibration of amine groups beside the CH_2 stretching vibration observed at 2915 and 2849 cm^{-1} corresponding to the alkyl chain of EDA. Subsequently, aminooxy-acetyl groups were grafted according to the procedure reported by Zhang et al. (Zhang et al., 2013) using Boc-aminooxyacetic acid. Deprotection of the aminooxy groups was achieved with HCl. D-Fructose 6-phosphate was covalently bonded to oxyamino group to form a stable link. FT-IR and contact angle were achieved to follow biolayer formation. The attachment of F6P carbohydrate was well observed thanks to amide link which provided two vibrations of amide I and amide II at respectively 1645 and 1550 cm^{-1} corresponding to the amide link with terminated surface and an intense band at 3200 cm^{-1} corresponding to various OH vibrations present in carbohydrate (See Supp. Info. SI.1–2, Fig. S1-5). The further step involved blocking the non-reactive oxyamino groups with the alkyl chain of pentanoic acid. SEM and AFM images were recorded to analyze the topological surface of biosensors (see Supp. Info. SI.1–2, Fig. S1-6). Images show a compact surface after biolayer formation due to organic dense surface of the biosensor.

Characterization of the surface properties after such modification was studied through electrochemical impedance spectra recorded after various steps of biolayer formation. These were performed by measuring the interfacial properties of the layers following charge transfer of the redox probe $[Fe(CN)_6]^{4-}/[Fe(CN)_6]^{3-}$ from the solution to the surface (See Supp. Info. SI.1–2, Table S1). Thus, EIS measurement provides details in the kinetics of charge transfer through the sensing layer occurring at the electrode and gives information about the surface

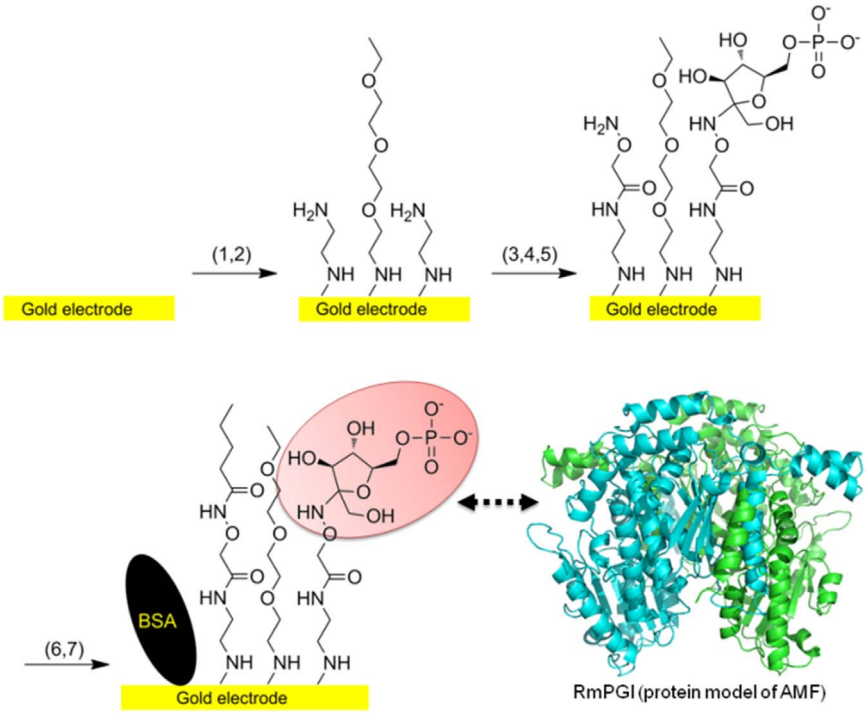

Fig. 1. Construction of the F6P-biosensor: (1)electrodeposition of ethylene diamine (EDA); (2) electrodeposition of polyethylene glycol substituted by an amine terminal group (PEG–NH_2); (3) grafting of 2-(*tert*-butoxycarbonylaminooxy) acetic acid; (4) deprotection with HCl; (5) grafting of F6P through oxime bond formation; (6) grafting of pentanoic acid; (7) blocking by bovine serum albumin (BSA).

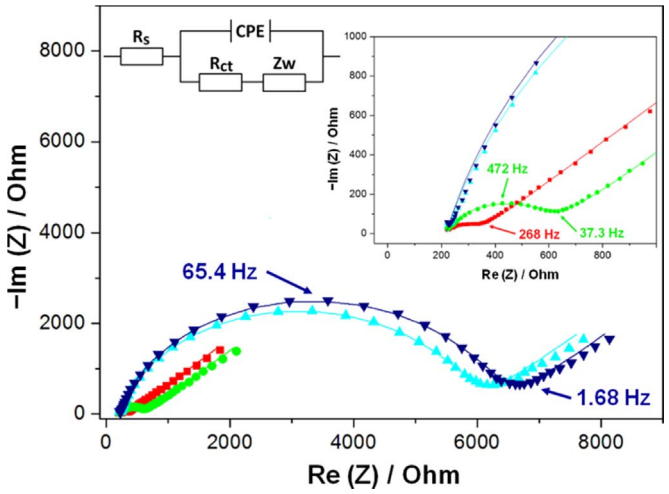

Fig. 2. Nyquist diagrams of the gold electrode following biosensor construction: step 2 (■), step 4 (•), step 5 (▲), and step 7 (▼) recorded in PBS with 5 mM $[Fe(CN)_6]^{4-}$/$[Fe(CN)_6]^{3-}$ species at potential 0.0 V vs Ag/AgCl and with Dc potential of 10 mV using a frequency range from 100 kHz to 0.1 Hz. The symbols are the experimental data and solids are the fitted curves using the Randles equivalent circuit model (R_s: electrolyte resistance, R_{ct}: charge transfer resistance, CPE: constant phase element, Zw: Warburg impedance). Enlarged view (0–1000 Ω) in inset.

modification and complex formation. Fig. 2 shows the Nyquist plots obtained after various steps of such surface modification. It is clear that modification of gold with the organic layer leads the increase of diameter of Nyquist plot. This increase, obtained after each step of the biolayer formation, is related to the increase of charge transfer resistance due to the blocking effect provided by the various molecules attached on the surface. This increase is important when the bioreceptor D-fructose 6-phosphate was attached to the surface. This could be related to the negative charge of the phosphate groups leading to electrostatic repulsion with the negatively charged redox probe $[Fe(CN)_6]^{4-}$/$[Fe(CN)_6]^{3-}$. In order to avoid non-specific interactions, pentanoic acid was used in the last step for blocking the non-functionalized oxyamino groups, and bovine serum albumin to block all the pinhole on the surface. Comparison of the electrochemical impedance spectra recorded following blocking of the surface with BSA (Fig. 2) shows small modification. This is due to a small interaction of BSA with the surface as the first steps involved deposition of ethylene glycol which blocks most pinholes on gold surface. EIS data were fitted satisfactory by a Randles equivalent circuit model (see inset in Fig. 2) where R_s is electrolyte resistance, R_{ct} is charge transfer resistance, capacitance is replaced by constant phase element (CPE), and Zw is Warburg impedance. Stepwise surface modification was also followed by cyclic voltammetry measurement and gave results in accord with EIS measurement (See Supp. Info. SI.1–2, Fig. S1-7).

3.2. Properties of F6P-biosensor in PBS

Detection of the protein was performed in the range of concentrations from 10 fM to 100 nM. For this purpose, the biosensor was dipped into the buffer containing various concentrations of enzyme. The F6P–protein interaction was analyzed by SWV (Fig. 3A) and EIS (Fig. 3B) in $[Fe(CN)_6]^{4-}$/$[Fe(CN)_6]^{3-}$ solution. Fig. 3A shows that the peak current corresponding to the redox signal of $[Fe(CN)_6]^{4-}$/$[Fe(CN)_6]^{3-}$ decreases upon increasing enzyme concentration. This could be related to the decrease of electron transfer that occurs from the solution to the electrode surface, due to changes of sensor properties caused by protein binding.

The Nyquist plots depicted in Fig. 3B give the same behavior where impedances increase after F6P–protein complex formation. As demonstrated by the error value (See Supp. Info. SI.2–1, Table S2), EIS data were fitted satisfactory by the Randles equivalent circuit model shown in inset and presented previously. The ESI measurement shows an increase of R_{ct} upon increasing of enzyme concentration in accordance with SWV results. This demonstrates variation of the permeability of the sensing layer upon attachment of a large molecule onto the surface which affects charge transfer resistance. Detection of protein is based on the lower permeation of redox markers to the surface of the

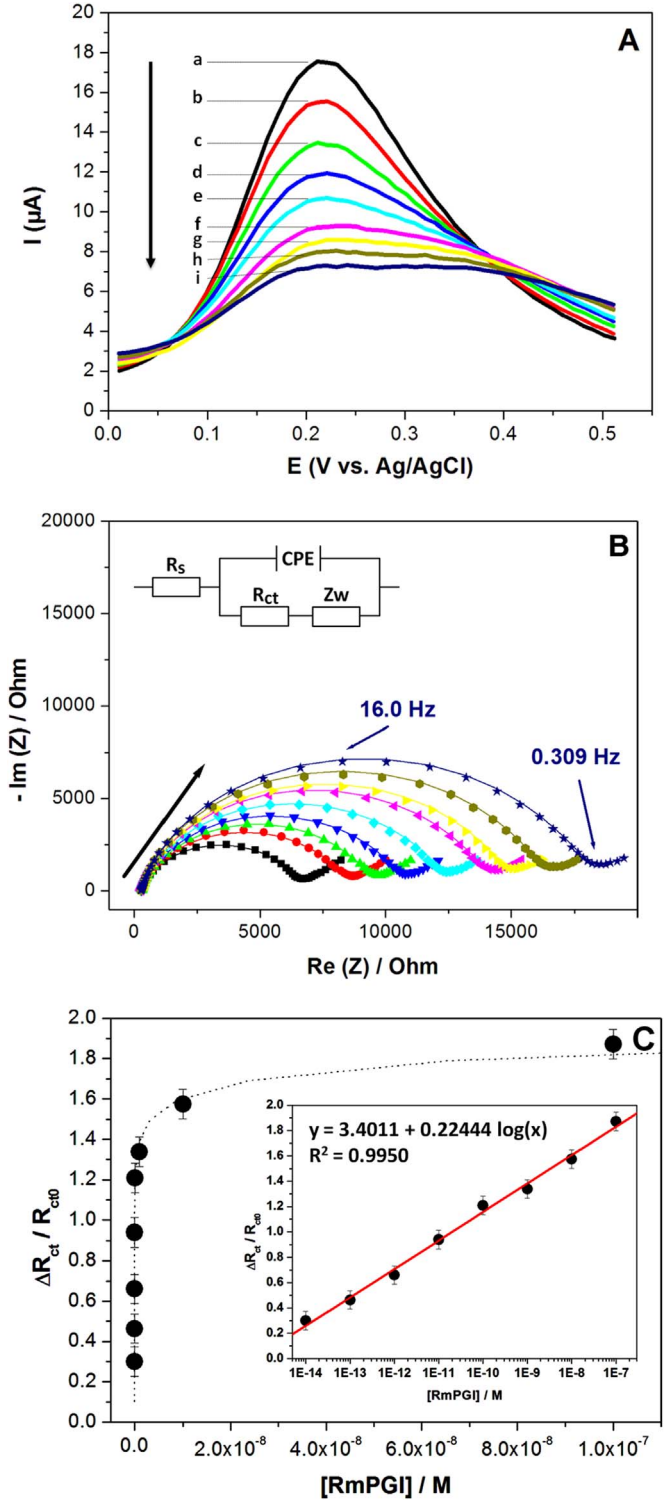

Fig. 3. (A) SWV obtained with modulation amplitude of 20 mV and frequency of 25 Hz after protein interaction with RmPGI concentration from top to bottom: biosensor alone (a), 10 fM (b), 100 fM (c), 1 pM (d), 10 pM (e), 100 pM (f), 1 nM (g, 10 nM (h), 100 nM (i). (B) Nyquist plots of the RmPGI biosensor response performed in the same condition as previously (■: biosensor alone, •: 10 fM, ▲: 100 fM, ▼: 1 pM, ◆: 10 pM, ◄: 100 pM, ►: 1 nM, ⬢: 10 nM, ⋆: 100 nM). The symbols are the experimental data and solids are the fitted curves using the equivalent circuit model shown in inset and described previously. (C) Calibration curve obtained from ESI data of the F6P-biosensor as a function of RmPGI concentration. Error bars represents the standard deviation across four independent measurements. The inset shows the calibration curve as a function of protein concentration (logarithmic scale).

electrode where formation of the complex prevents electronic communication with the gold surface (Miodek et al., 2013). This behavior is amplified by dense carbohydrate monolayer surface. Less density of carbohydrates leads to small variation of the response signal and then less sensitivity of the biolayer to low concentration of proteins.

The calibration curve could be obtained through measurement of the variation of R_{ct} upon protein concentration (Fig. 3C) and standard deviation for each measurement was determined with four independent measurements. R_{ct} shows a good linear correlation (R^2=0.9950) with the logarithmic scale of PGI concentration from 10 fM to 100 nM. Variation of current intensity of the redox probe upon concentration of PGI gives a variation in a rather large concentration range of 100 nM in logarithmic scale (See Supp. Info. SI.2–1, Fig. S2–1). This demonstrates the ability of ESI to perform such analytic experiment (Tlili et al., 2008). The regression equation was $\Delta R_{ct}/R_{ct0}$ =0.22444 log [PGI] +3.4011, and the detection limit was calculated to be 6.6 fM based on a signal-to-noise ratio of 3 and taking into account the standard deviation across four independent measurements obtained for the lower value measured.

To explain the low detection limit obtained, the affinity constant of F6P to the enzyme was measured. In the same way, the affinity of the derivative of F6P modified by a methyloxime group on C-2 (Wieczorek, 2010) to mimic the lateral chain attached to biosensor (See Supp. Info. SI.2–1, Scheme S1) was measured following standard procedures for competitive binding assays on PGI (Hardré and Salmon, 1999). The affinity constant of F6P methyloxime is about 40 µM and shows higher affinity than F6P (100 µM). The affinity constants are measured in solution where F6P is predominantly in cyclic form. On the contrary, the methyloxime derivative of F6P in solution is predominantly in linear form (Wieczorek, 2010). Immobilization on the surface could indeed provide a favorable linear geometry of the F6P bioreceptor. This hypothesis is further confirmed by the known better affinity of linear PGI inhibitors over cyclic PGI inhibitors (Hardré, 2001). However, the affinity constant obtained in solution is clearly not the only parameter that explains efficiency of the protein attachment to the surface and complex formation. Successful macromolecular organization on the electrode surface as well as the method of measurement could also improve sensitivity of the biosensor. Thus apparent affinity constant of F6P/PGI obtained on the surface could be estimated through the curve variation of signal (S) with protein concentration [PGI] (See Supp. Info. SI.2–1, Fig. S2–2). This curve could be fitted by the Langmuir-Freundlich model to provide the value of apparent affinity constant K_{app} on the surface with the equation:

$$\frac{1}{S} = \frac{1}{S_{max}} + \frac{1}{K_{app} S_{max}[PGI]}$$

The fitting gives a K_{app} value of 4.4 ± 1.4 nM which is very low compared to the value obtained with competitive assay. Thus it is well known that immobilization on the surface affects conformational and rotational behaviors of proteins and their complexes. In addition, binding of protein is sensitive to chemical and physical environment such as hydrophobic or ionic character. Thus F6P anchoring through oxime ligation, beside the surface structure of the biosensor negatively charged provided by octanoic acid and hydrophilic character obtained by attached PEG as demonstrated previously, favors protein interaction with the F6P monosaccharide. Molecular modeling studies under investigation could give more information about protein amino acids involved in such interaction.

3.3. Specificity of F6P-biosensor in PBS

Protein specificity of the F6P-biosensor for RmPGI was confirmed through study of biosensor properties towards another sugar enzyme,

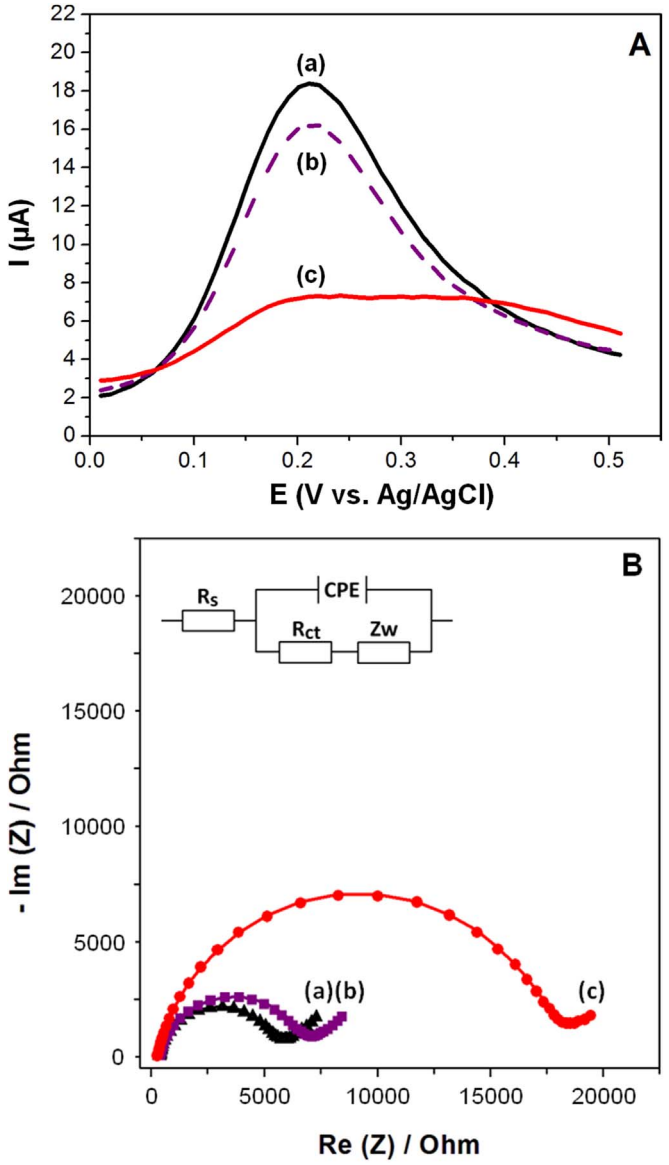

Fig. 4. (A) SWV and (B) Nyquist plots obtained with the same conditions as previously (the symbols are the experimental data and solids are the fitted curves using the equivalent circuit model shown in inset and described previously): (a) biosensor alone, (b) with ScG6PDH 100 nM, (c) with RmPGI 100 nM.

namely D-glucose-6-phosphate dehydrogenase from *Saccharomyces cerevisiae* (ScG6PDH). G6PDH reacts specifically on D-glucose 6-phosphate, a phosphorylated carbohydrate which structure most closely resembles F6P. The biosensor was incubated in a highly concentrated solution of ScG6PDH (100 nM) in the same conditions as for RmPGI. After washing step, SWV and ESI were measured. Fig. 4A shows SWV where a weak decrease of the current intensity corresponding to −11% was obtained compared to the same concentration of PGI with a variation of −60%. Nyquist plots shown in Fig. 4B demonstrate the same behavior. Considering the R_{ct} values recorded in absence of RmPGI and ScG6PDH, respectively 6.119 kΩ and 5.164 kΩ (Supp. Info. SI.2–2, Table S3), the biosensor response for 100 nM ScG6PDH (6.269 kΩ) could be classified as noise. With a concentration of ScG6PDH lower than 1 nM, no variation is obtained. These results underline the non-specific interaction of this enzyme. The F6P-functionalized gold electrode appears highly specific for RmPGI, a protein model of the cytokine AMF.

The reproducibility of biosensors was studied by measuring four independent measurements with fresh biosensors. Relative standard deviation of less than 5% was calculated. Stability of the biosensor was tested within four independent measurements. It was achieved by immersing the electrode in buffer solution during 10 h and the response of the biosensor at various times were recorded. Results show no modification of the signal, which demonstrates high stability of the four biosensors (See Supp. Info. SI.2–3, Fig. S2–3).

3.4. Properties and specificity of F6P-biosensor in human plasma

Detection of RmPGI was further performed in human plasma in the range of concentrations varying from 1 fM to 10 pM. The carbohydrate-protein interaction was analyzed by SWV and EIS in $[Fe(CN)_6]^{4-}$/$[Fe(CN)_6]^{3-}$ solution, as previously described in PBS, using one electrode only. The Nyquist plots reported in Supp. Info. SI.3 (Figs. S3–1) give a similar behavior as in PBS where impedances increase after F6P–RmPGI complex formation. The calibration curve could be obtained by measurement of R_{ct} upon protein concentration (see Supp. Info. SI.3, Table S4). Smaller R_{ct} values were recorded in human plasma than in PBS most likely because of the medium change. Human plasma is quite different from the PBS and lower diffusion coefficients and kinetic constant should be expected and, thereof, lower R_{ct} values. However, R_{ct} shows a good linear correlation (R^2=0.9810) with the logarithmic scale of RmPGI concentration from 1 fM to 10 pM. The regression equation was $\Delta R_{ct}/R_{ct0}$ =0.19671 log[RmPGI] +3.4011, and the detection limit was calculated to be 113 fM based on a signal-to-noise ratio of 3 and taking into account the standard deviation obtained from the linear regression curve (0.20447). Although sensitivity of the F6P-biosensor is lower in human plasma than in PBS, most likely because the sample contains a complex mixture of molecules, LD is still in the low picomolar range. Incubation of the biosensor in human plasma spiked with ScG6PDH at concentrations of 100 fM, 100 pM and 100 nM induces almost no variation of the square wave voltammograms (see Supp. Info. SI.3, Figs. S3–2), demonstrating high-specificity of the F6P-biosensor for RmPGI in human plasma. Recovery rates calculated for the detection of RmPGI in human plasma versus PBS varied from 112% at 10 pM to 131% at 10 fM. These values most likely originates from matrice effects due to undiluted and unfiltered human plasma (see Supp. Info. SI.3, Table S5).

3.5. Comparison of sensing performances

Detection of cancer biomarkers in human tissues and fluids is the subject of intense research and has been thoroughly reviewed (Bohunicky and Mousa, 2010; Chikkaveeraiah et al., 2012; Li et al., 2012; Tothill, 2009; Yang et al., 2014). However, biosensors designed for the detection of cancer biomarkers of clinical interest are quasi-exclusively immunosensors (Wang et al., 2008; Jie et al., 2010; Lin et al., 2011; Zhang et al., 2012; Hao et al., 2012; Tang et al., 2014; Ali et al., 2015; W. Wang et al., 2015a,2015b), which could be cost-effective for some of them. Despite the fact that our F6P-biosensor uses affordable reagents for its design, its sensing performances are remarkably high when compared to reported electrochemical immunosensors in term of LD and linear range (Table 1). Regarding only AMF, known enzymatic (Gracy and Tilley, 1975), colorimetric (Bodansky, 1954b), and immunological (Dai et al., 2010; Dobashi et al., 2006; Fan et al., 2010) methods used for quantification of the protein in human fluids are adapted for concentrations in the pM to nM range, well above the F6P-biosensor femtomolar range of detection. Most importantly, we report the first electrochemical biosensor designed for the detection of a protein model of AMF. Because a confident prognosis generally requires the detection of several cancer biomarkers, our study might afford a valuable contribution to minimize false-positive responses in prognosis of cancer.

In addition, only a few electrochemical carbohydrate-based biosensors designed for the detection of sugar-binding proteins were reported in the literature (Zhang et al., 2013; Gruber et al., 2011; Huang et al.,

Table 1
Comparison of sensing performances for the electrochemical detection of selected cancer biomarkers in clinical use.[a].

Bio-marker	Cancer type	Detection method	Linear range	LD (pg mL^{-1})	LD (fM)	Materials used/epitope linked	Reference
BRCA1	Breast	EIS	50 fM–1.0 nM	–	1.72	AuNP/PEG-ssDNA	(W. D Wang et al., 2015; W Wang et al., 2015)
ErbB2	Breast	EIS	1.0 fM–500 nM	–	1.0	ZnOnF/anti-ErbB2	(Ali et al., 2015)
PSA	Prostate	DPV	–	6	–	AuPD/Ab1	(Tang et al., 2014)
		ECL	0.001–50 ng/mL	0.6	–	CNT-Chitosan-AuNP/Ab1	(Zhang et al., 2012)
CEA	several	ECL	0.05–200 ng/mL	10	–	CdTe-QD	(Jie et al., 2010)
			0.005–0.35 pg/mL	0.002	–	$Ru(bpy)_3^{2+}$-GN/Ab1-QD	(Hao et al., 2012)
AFP	several	ECL	0.14 fM–14 pM	0.001	0.014	AuNP/Ab2-DNA-hemin	(Lin et al., 2011)
p53	several	CV	2.2 pM–5.6 nM	120	2200	AuNW/ODN-AuNP-Strep	(Wang et al., 2008)
AMF	several	EIS-SWV	10 fM–100 nM	0.09	0.7	Au/PEG-F6P	our study

[a] AFP: Alpha-fetoprotein, CEA: Carcinoembryonic antigen, CNT: Carbon nanotube, CV: cyclic voltammetry, DPV: differential pulse voltammetry, ECL: Electrochemiluminescence, EIS: electrochemical impedance spectroscopy, GN: Graphene-Nafion, LD: limit of detection, NP: nanoparticules, nF: nanofibers, PD: paper disk, QD: Quantum dots, Strep: streptavidine, SWV: square wave voltammetry.

2015; Guo et al., 2012). Most of them are based on lectins detection. Not only is our electrochemical F6P-biosensor one of the few biosensors with remarkable sensing performances designed for the detection of a non-lectin sugar-binding protein, but also is, as far as we know, the first biosensor ever reported developed for the detection of a phosphate-sugar-binding protein. In addition our biosensor performance is obtained with direct way without the amplification step which facilitates its application in real samples such as plasma.

4. Conclusions

In conclusion, we report in this study the construction, characterization and evaluation of the first electrochemical biosensor designed for the detection and quantification of rabbit muscle phosphoglucose isomerase, a protein model of the cancer and potential metastatic biomarker AMF. The F6P-biosensor was elaborated by oxime bond formation between the RmPGI substrate F6P on its C-2 carbon, which proves well adapted, and a modified gold electrode bearing oxyamino groups. The designed biosensor shows high sensitivity towards RmPGI with a limit of detection in PBS at 6.6 fM (113 fM in human plasma) and wide range of detection between 10 fM and 100 nM (1 fM to 10 pM in human plasma). High specificity for RmPGI with rather no detection of the enzyme D-glucose-6-phosphate dehydrogenase from *S. cerevisiae* was demonstrated in PBS, as well as in human plasma. Hence, the F6P-biosensor appears as a highly promising proof of concept for the future development of an electrochemical device that would allow rapid and reliable quantification of the cytokine AMF in human fluids. To our knowledge, and although much remains to do, such a device would be the first analytical tool allowing easy, early and efficient detection of an on-going metastatic process in cancer patients.

Author contributions

The manuscript was written through contributions of all authors.

Notes

The authors declare no competing financial interest.

Acknowledgement

This work was supported by CNRS following the project “Défi Instrumentation aux Limites” FLUTRACE (Grant No. 44704). Authors acknowledge Hélène Dorizon for providing 2-[2-(2-ethoxyethoxy) ethoxy]-ethylamine (PEG–NH_2), and Florence Wieczorek and Philippe Durand (ICSN, Gif-sur-Yvette) for providing F6P methyloxime.

Appendix A. Supporting information

Supplementary data associated with this article can be found in the online version at doi:10.1016/j.bios.2017.04.031.

References

Adenier, A., Chehimi, M.M., Gallardo, I., Pinson, J., Vilà, N., 2004. Langmuir 20, 8243–8253.
Ali, M.A., Mondal, K., Singh, C., Malhotra, B.D., Sharma, A., 2015. Nanoscale 7, 7234–7245.
Alliband, A., Meece, F.A., Jayasinghe, C., Burns, D.H., 2013. J. Org. Chem. 78, 356–362.
Baumann, M., Brand, K., 1988. Cancer Res. 48, 7018–7021.
Baumann, M., Kappl, A., Lang, T., Brand, K., Siegfried, W., Paterok, E., 1990. Cancer Investig. 8, 351–356.
Bayo, J., Fiore, E., Aquino, J.B., Malvicini, M., Rizzo, M., Peixoto, E., Andriani, O., Alaniz, L., Piccioni, F., Bolontrade, M., Podhajcer, O., Garcia, M.G., Mazzolini, G., 2014. PLoS One 9, e95171.
Bodansky, O., 1954a. Cancer 7, 1200–1226.
Bodansky, O., 1954b. Cancer 7, 1191–1199.
Bohunicky, B., Mousa, S.A., 2010. Nanotechnol. Sci. Appl. 4, 1–10.
Brooks, J.D., 2012. Genome Res. 22, 183–187.
Chikkaveeraiah, B.V., Bhirde, A.A., Morgan, N.Y., Eden, H.S., Chen, X., 2012. ACS Nano 6, 6546–6561.
Chiu, C., St-Pierre, P., Nabi, I., Wiseman, S., 2008. Expert Rev. Anticancer Ther. 8, 207–217.
Dai, L., Zhu, L.-J., Zheng, D.-H., Mo, Y.-Q., Wei, X.-N., Su, J.-H., Pessler, F., Zhang, B.-Y., 2010. J. Rheumatol. 37, 2452–2461.
Dobashi, Y., Watanabe, H., Matsubara, M., Yanagawa, T., Raz, A., Shimamiya, T., Ooi, A., 2006. J. Pathol. 208, 44–53.
Dong, H., Li, C.M., Chen, W., Zhou, Q., Zeng, Z.X., Luong, J.H.T., 2006. Anal. Chem. 78, 7424–7431.
Dyson, J.E.D., Noltman, E.A., 1968. J. Biol. Chem. 243, 1401–1414.
Fan, L.Y., Zong, M., Wang, Q., Yang, L., Sun, L.S., Ye, Q., Ding, Y.Y., Ma, J.W., 2010. Clin. Chim. Acta 411, 2049–2053.
Filella, X., Molina, R., Jo, J., Mas, E., Ballesta, A.M., 1991. Tumour Biol. 12, 360–367.
Funasaka, T., Haga, A., Raz, A., Nagase, H., 2001. Biochem. Biophys. Res. Commun. 285, 118–128.
Funasaka, T., Hu, H., Yanagawa, T., Hogan, V., Raz, A., 2007. Cancer Res. 67, 4236–4243.
Füzéry, A.K., Levin, J., Chan, M.M., Chan, D.W., 2013. Clin. Proteom. 10, 13.
Gerlach, J.Q., Cunningham, S., Kane, M., Joshi, L., 2010. Biochem. Soc. Trans. 38, 1333–1336.
Gong, W., Jiang, Y., Wang, L., Wei, D., Yao, J., Huang, S., Fang, S., Xie, K., 2005. Clin. Cancer Res. 11, 5778–5783.
Gracy, R.W., Tilley, B.E., 1975. [84] Phosphoglucose isomerase of human erythrocytes and cardiac tissue. In: Wood, W.A. (Ed.), Methods Enzymol., Carbohydrate Metabolism, Part B. Academic Press, 392–400.
Gruber, K., Horlacher, T., Castelli, R., Mader, A., Seeberger, P.H., Hermann, B.A., 2011. ACS Nano 5, 3670–3678.
Guirguis, R., Schiffmann, E., Liu, B., Birkbeck, D., Engel, J., Liotta, L., 1988. J. Natl. Cancer Inst. 80, 1203–1211.
Guo, X., Kulkarni, A., Doepke, A., Halsall, H.B., Iyer, S., Heineman, W.R., 2012. Anal. Chem. 84, 241–246.
Haga, A., Funasaka, T., Niinaka, Y., Raz, A., Nagase, H., 2003. Int. J. Cancer 107, 707–714.
Haga, A., Tanaka, N., Funasaka, T., Hashimoto, K., Nakamura, K.T., Watanabe, H., Raz, A., Nagase, H., 2006. J. Mol. Biol. 358, 741–753.
Hao, T., Guo, Z., Du, S., Shi, L., 2012. Sens. Actuators B-Chem. 171–172, 803–809.
Hardré, R., 2001. (Ph.D. thesis). Université Paris-Sud (Orsay, France).

Hardré, R., Salmon, L., 1999. Carbohydr. Res. 318, 110–115.
Huang, L.-D., Adak, A.K., Yu, C.-C., Hsiao, W.-C., Lin, H.-J., Chen, M.-L., Lin, C.-C., 2015. Chem. Eur. J. 21, 3956–3967.
Huang, Z., Zhang, N., Zha, L., Mao, H.-C., Chen, X., Xiang, J.-F., Zhang, H., Wang, Z.-W., 2014. Asian Pac. J. Cancer Prev. 15, 989–997.
Iizumi, M., Liu, W., Pai, S.K., Furuta, E., Watabe, K., 2008. Biochim. Biophys. Acta 1786, 87–104.
Jeffery, C.J., 1999. Trends Biochem. Sci. 24, 8–11.
Jiang, W., Raz, A., Douglas-Jones, A., Mansel, R., 2006. J. Histochem. Cytochem. 54, 231–241.
Jie, G.-F., Liu, P., Zhang, S.-S., 2010. Chem. Commun. 46, 1323–1325.
Lagana, A., Duchaine, T., Raz, A., DesGroseillers, L., Nabi, I.R., 2000. Biochem. Biophys. Res. Commun. 273, 213–218.
Lagana, A., Goetz, J.G., Altschuler, Y, Y., N., Nabi, I.R., 2005. J. Cell. Sci. 118, 4175–4185.
Lee, J.H., Chang, K.Z., Patel, V., Jeffery, C.J., 2001. Biochemistry 40, 7799–7805.
Li, C.M., Chen, W., Yang, X., Sun, C.Q., Gao, C., Zheng, Z.X., Sawyer, J., 2005a. Front. Biosci. 10, 2518–2526.
Li, C.M., Sun, C.Q., Song, S., Choong, V.E., Maracas, G., Zhang, X.J., 2005b. Front. Biosci. 10, 180–186.
Li, J., Li, S., Yang, C.F., 2012. Electroanalysis 24, 2213–2229.
Lin, D., Wu, J., Yan, F., Deng, S., Ju, H., 2011. Anal. Chem. 83, 5214–5221.
Liotta, L.A., Mandler, R., Murano, G., Katz, D.A., Gordon, R.K., Chiang, P.K., Schiffmann, E., 1986. Proceedings Natl. Acad. Sci. USA 83, 3302–3306.
Miller, A.D., Keller, M., Jorgensen, M., Perouzel, E., 2005. U.S. Pat. Appl. Publ. US0287202 A1.
Miodek, A., Castillo, G., Hianik, T., Korri-Youssoufi, H., 2013. Anal. Chem. 85, 7704–7712.
Noltmann, E.A., 1964. J. Biol. Chem. 239, 1545–1550.
Paschos, K.A., Canovas, D., Bird, N.C., 2009. Hippokratia 13, 23–31.
Patel, P.S., Raval, G.N., Rawal, R.M., Patel, G.H., Balar, D.B., Shah, P.M., Patel, D.D., 1995. Neoplasma 42, 271–274.
Reichardt, N.C., Martín-Lomas, M., Penadés, S., 2013. Chem. Soc. Rev. 42, 4358–4376.
Sánchez-Pomales, G., Zangmeister, R.A., 2011. Int. J. Electrochem. 825790, 1–11.
Schwartz, M.K., Greenberg, M.D., Bodansky, O., 1963. Cancer 16, 583–594.
Takanami, I., Takeuchi, K., Naruke, M., Kodaira, S., Tanaka, F., Watanabe, H., Raz, A., 1998. Tumour Biol. 19, 384–389.
Talukder, A.H., Adam, L., Raz, A., Kumar, R., 2000. Cancer Res. 60, 474–480.
Tang, C.K., Vaze, A., Rusling, J.F., 2014. Anal. Methods 6, 8878–8881.
Tlili, C., Jaffrezic-Renault, N., Martelet, C., Mahy, J.P., Lecomte, S., Chehimi, M.M., Korri-Youssoufi, H., 2008. Mater. Sci. Eng. C, MADICA 2006 Conference, In: Proceedings of the Fifth Maghreb-Europe Meeting on Materials and their Applicatons for Devices and Physical, Chemical and BiologicalSensorsMADICA 2006 Conference, Fifth Maghreb-Europe Meeting on Materials and their Applicatons for Devices and Physical, Chemical and BiologicalSensors 28, 861–868.
Torimura, T., Ueno, T., Kin, M., Harada, R., Nakamura, T., Kawaguchi, T., Harada, M., Kumashiro, R., Watanabe, H., Avraham, R., Sata, M., 2001. Hepatology 34, 62–71.
Tothill, I.E., 2009. Semin. Cell. Dev. Biol. A Spec. Ed. Biosens. Dev. Pigment Cells Pigment Patterns 20, 55–62.
Tsutsumi, S., Yanagawa, T., Shimura, T., Kuwano, H., Raz, A., 2004. Clin. Cancer Res. 10, 7775–7784.
Tsutsumi, S., Fukasawa, T., Yamauchi, H., Kato, T., Kigure, W., Morita, H., Asao, T., Kuwano, H., 2009. Int. J. Oncol. 35, 1117–1121.
Wang, D., Hu, W., Xiong, Y., Xu, Y., Ming Li, C., 2015a. Biosens. Bioelectron. 63, 185–189.
Wang, J., Zhu, X., Tu, Q., Guo, Q., Zarui, C.S., Momand, J., Sun, X.Z., Zhou, F., 2008. Anal. Chem. 80, 769–774.
Wang, W., Fan, X., Xu, S., Davis, J.J., Luo, X., 2015b. Biosens. Bioelectron. 71, 51–56.
Watanabe, H., Carmi, P., Hogan, V., Raz, T., Silletti, S., Nabi, I.R., Raz, A., 1991. J. Biol. Chem. 266, 13442–13448.
Watanabe, H., Takehana, K., Date, M., Shinozaki, T., Raz, A., 1996. Cancer Res. 56, 2960–2963.
Wieczorek, F., 2010. Les oximes dans la recherche d'inhibiteurs de la glucosamine-6P Synthase: synthèses, études physico-chimiques et évaluations in vitro (PhD thesis). Univ Paris-Sud, Orsay, France.
Yanagawa, T., Funasaka, T., Tsutsumi, S., Watanabe, H., Raz, A., 2004. Endocr. -Relat. Cancer 11, 749–759.
Yang, M., Yi, X., Wang, J., Zhou, F., 2014. Analyst 139, 1814–1825.
Zhang, G.-J., Huang, M.J., Ang, J.J., Yao, Q., Ning, Y., 2013. Anal. Chem. 85, 4392–4397.
Zhang, M., Dai, W., Yan, M., Ge, S., Yu, J., Song, X., Xu, W., 2012. Analyst 137, 2112–2118.